Journal of the European Ceramic Society **18** (1998) 1797–1808

PII: S0955-2219(98)00119-8
0955-2219/98/$—see front matter

Probabilistic-statistical Approach to Matrix Damage and Stress–Strain Behavior of 2-D Woven SiC/SiC Ceramic Matrix Composites

J. Lamon,* B. Thommeret and C. Percevault

Laboratoire des Composites Thermostructuraux, UMR 47 (CNRS-SEP-UBl), Domaine Universitaire, 3 Allée de La Boétie, 33600 Pessac, France

Abstract

The matrix damage evolution in a 2-D SiC/SiC composite reinforced with fabrics of fiber bundles was predicted from properties of basic constituents using a finite element analysis of failure probabilities. Failure probabilities were computed using a finite element post processor including the multiaxial elemental strength model for handling fracture statistics under multiaxial stress-states. The associated stress–strain behavior of the selected elementary cell was derived from the stress analysis. The predicted matrix damage evolution was found in good agreement with that identified by microscopy on practical 2-D SiC/SiC woven composites under tension. The predicted stress–strain behavior and Young's moduli compared satisfactorily with the experimental data. The approach was then applied to a cell of fully dense 2-D woven SiC/SiC composite under tension, and then to a cell of conventional 2-D woven SiC/SiC composite subject to a gradient of forces.

Keywords: fracture probability, finite element analysis, SiC/SiC, woven reinforcement, matrix cracking, stress–strain behavior

1 Introduction

Ceramic matrix composites (CMCs) combine brittle ceramic materials, i.e. the fibers and the matrix. Nevertheless they are capable of a highly non-linear stress–strain behavior reflecting the accommodation of deformations and a damage tolerance. These features involve multiple microcracks or cracks that form in the matrix and then are arrested by the fibers. The matrix cracks and the associated debonds affect locally the stress field operating on the fibers. Individual fiber breaks occur first. The ultimate failure occurs when a critical number of fibers have failed.

Formation of matrix cracks and fiber failures are random brittle failure phenomena, as a result of the presence of populations of fracture inducing flaws distributed randomly in the matrix and in the fibers.

Fracture-statistical based approaches are appropriate for modeling the defect-induced failures of brittle materials. Several approaches to brittle fracture have been proposed in the literature. The Weibull model provides a satisfactory approximation in the presence of uniaxial stress states. More fundamental approaches such as the multiaxial elemental strength model are required for multiaxial stress states and complex shapes.[1–4] Damage and failure models based upon statistical approaches to brittle failure have been developed to predict the ultimate strength,[5–8] and the stress–strain behavior[9,10] of unidirectionally reinforced CMCs subject to tensile loads, including microcomposites (elementary scale)[9] and minicomposites (intermediate scale).[10] A microcomposite consists of a concentric cylinder element containing a single fiber with a coating (i.e. interphase) plus a matrix annulus, whereas a minicomposite contains a fiber tow.

In the composites reinforced with fabrics of fiber bundles the matrix damage is influenced by the microstructure.[11] The 2-D SiC/SiC made by chemical vapor infiltration (CVI) of a fiber preform displays a highly heterogeneous microstructure (Fig. 1) consisting of woven infiltrated tows that behave as physical entities, large pores (referred to as macropores) located between the plies or at yarn intersections within the plies, and a uniform layer of matrix over the fiber preform (referred to as the intertow matrix). Much smaller pores are also present within the tows. Extensive inspection of the composite under a tensile load using a microscope

*To whom correspondence should be addressed.

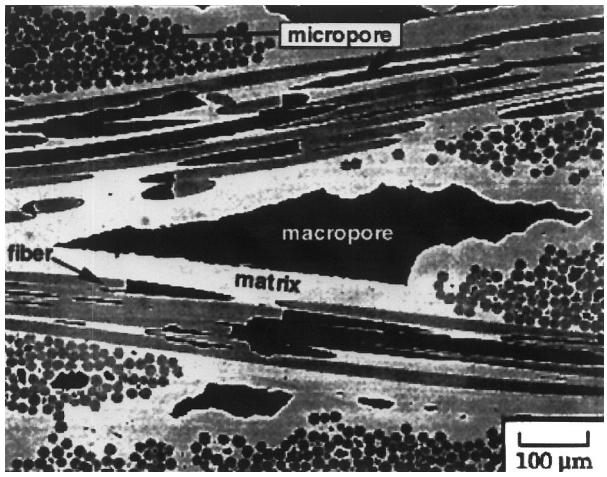

Fig. 1. Microstructure of the 2-D woven SiC/SiC composite made by chemical vapor infiltration.[11]

has shown that matrix cracking affects first the intertow matrix, then the transverse infiltrated tows and finally the longitudinal infiltrated tows.[11]

Much attention has been given to the prediction of the stress–strain behavior of multidirectionally reinforced CMCs and particularly the 2-D SiC/SiC composites.[12–15] The approaches can be grouped into two categories:

- the micromechanics-based approaches, aimed at predicting the stress-strain behavior from the constituent properties and,
- the damage mechanics-based approaches, that consider the composite as a continuous medium at the macroscopic or at an intermediate mesoscopic scale.

Most approaches and particularly those based upon damage mechanics, require data measured on the current composite. Therefore, they can be applied solely to fabricated materials. They cannot be used for composite design. Approaches based upon constituent properties seem to be more appropriate for this purpose. Previous work[11,15] has demonstrated that the non-linear stress–strain behavior of a two-dimensional woven composite may be predicted from constituent properties. The microstructure and the successive steps of matrix damage identified experimentally during tensile tests were duplicated in the finite element mesh for the prediction of the non-linear stress–strain behavior of a 2-D SiC/SiC composite.

The present paper proposes an alternative approach to the prediction of the stress–strain behavior from properties of basic constituents. This approach is based upon a finite element analysis to derive failure probabilities for the simulation of the matrix damage evolution. This probabilistic-statistical approach recognizes the random-defect induced aspect of cracking in brittle matrices. A cell of 2-D SiC/SiC composite under uniaxial tension was examined first. The approach was validated by comparing the simulated matrix cracking process with the sequence identified experimentally, and the corresponding stress–strain behavior with experimental results. Then, this approach was applied to a cell of 2-D SiC/SiC composite under bending conditions, and to a cell of fully dense 2-D SiC/SiC under uniaxial tension.

2 Simulation of Matrix Damage and Prediction of the Stress–Strain Relation

2.1 Determination of failure probabilities

First, stresses in the matrix are computed using a finite element code (MARC produced by MARC analysis). Then, failure probabilities are determined using the FLAG post processor developed by Lamon and Inghels. FLAG uses the finite-element output (principal stresses), and a material data file including the statistical parameters pertinent to composite basic constituents. The FLAG program includes the multiaxial elemental strength model[1–4] for handling multiaxial fracture statistics. The multiaxial elemental strength model was developed to predict the failure of ceramic materials under various stress-states and geometries. It is based upon the premise that the pre-existing flaws in the material can be characterized by their flaw extension stress, or strength S (referred to as the elemental strength). The flaw distributions are thus described by the distribution in elemental strengths S. The failure probability is then derived from the distribution in S.

The failure probability of a volume element of matrix (i.e. a single FE mesh unit) is calculated using the following equation:

$$P_{\mathrm{v}} = 1 - \exp\left[-\int_{\mathrm{v}}\left(\frac{\sigma_1}{\sigma_{\mathrm{ov}}}\right) m_{\mathrm{v}} I_{\mathrm{v}}\left(m_{\mathrm{v}}, \frac{\sigma_2}{\sigma_1}, \frac{\sigma_3}{\sigma_1}\right) dV\right] \tag{1}$$

where P_{v} is failure probability, σ_1, σ_2 and σ_3 are the principal stresses ($\sigma_1 > \sigma_2 > \sigma_3$), m_{v} and σ_{ov} are the flaw strength parameters, V is the volume of the considered matrix element. The function I_{v} (–) is detailed elsewhere.[1,16] It depends upon the local principal stress field through a non-coplanar strain energy release rate criterion for crack extension.[1,3,16]

2.2 Principle of matrix cracking simulation

The applied deformation (or stress) is increased incrementally. At each increment, the stress-state

and the unit mesh failure probabilities are computed. A crack in the intertow matrix or in the matrix in the transverse tows (perpendicular to the loading direction), or a damaged zone in the matrix in the longitudinal tows (parallel to the loading direction) is introduced at the location of the maximum unit mesh failure probability when this computed failure probability reaches the value of 1, in order to represent definite events. The cracks are introduced in the mesh by iteratively splitting the nodes. The damaged zones are characterized by an effective Young's modulus according to the density of matrix cracks, in order to take into account the contribution of the debonded fibers in the deformations of these longitudinal tows.

The simulation of the matrix cracking evolution may be summarized as follows. The applied deformation (or stress) is increased by constant increments until the failure probability in one of the mesh elements reaches 1. At this stage, the node located at the boundary between the two mesh elements where the failure probability is maximum, is split into two nodes to simulate a crack. In a four node element mesh, each node is common to four elements, and each element is bounded by six elements. The node to be split is common to the mesh element where the probability is 1, and to that one with the largest failure probability. When the tip of a crack is located within the intertow matrix or within a transverse tow, the application of this criterion indicates that the node to be split at crack tip is located in the crack direction. When a crack reaches a longitudinal tow, the application of this criterion indicates that the node to be split is now located in the tow boundary. The crack extension thus occurs at the boundary of the tow, which is the most realistic crack path.[11] As indicated above, matrix cracking in the longitudinal tows is described by a decrease in the Young's modulus. After each step of node splitting or modulus decrease, the applied deformation (or stress) is kept constant, and the stresses (or strains) and the failure probabilities are computed. If the failure probability in one of the mesh elements is 1, one more node is splitted or the Young's modulus is decreased according to the previous failure probability based criterion. This procedure is repeated at constant deformation (or stress) until the unit mesh failure probabilities are smaller than 1. The applied deformation (or stress) is increased only once the computed failure probabilities are smaller than 1, and the procedure is iteratively repeated.

It is worth mentioning that no boundary condition was specified on matrix/tow interactions in the debonded regions. Obviously, this approach may simulate weak fiber/matrix interactions and lead to an underestimation of the resulting stress (or an overestimation of the resulting strain) at the boundary of the cell and of the cell Young's modulus. The matrix blocks which are delineated by four intersecting cracks are no longer bonded to the rest of the material. Therefore, they are discarded.

2.3 Derivation of the stress–strain curve

The overall average stress operating on a face of the considered cell is derived from the stresses computed at the nodes of this face at a given applied deformation (deformation-based analysis). The successive applied deformations and the associated overall average stresses provide the stress–strain curves and the cell effective Young's moduli at various damage steps. In the case when stresses instead of deformations are applied to the cell (stress-based analysis), the same method is employed to determine the mean strains, and then the stress–strain curve and the effective Young's moduli.

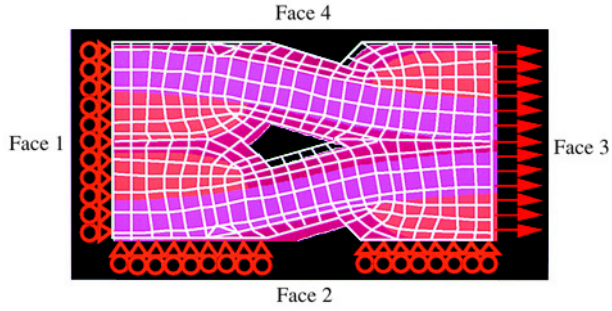

Fig. 2. Mesh used in the finite elements computations.

Table 1. Main mechanical properties of composite constituents

Constituents	*Young's modulus (GPa)*	*Poisson's ratio*
Fiber	200	0·25
Matrix	400	0·20
Longitudinal tows	260	0·20
Damaged longitudinal tows	100	0·25
Transverse tows	160	0·20

Table 2. Statistical parameters of the SiC matrix in the different constituents of the SiC/SiC composite

Constituents	*Weibull modulus*	*Scale factor (MPa)*
Microcomposite	4·9	1·6
Minicomposite	6·2	11·3
Interply matrix	4·9	1·6
Transverse tow matrix	4·9	0·66
Longitudinal tow matrix	6·2	7·3

2.4 Application to a 2-D SiC/SiC composite under tension and under bending

2.4.1 Mesh and boundary conditions

A 2-D elementary cell with 329 elements (Fig. 2) was constructed according to the microstructure and the ply arrangements observed on practical 2-D SiC/SiC CVI composites.[11] The most frequently encountered out-of-phase ply arrangement was duplicated in the mesh (Fig. 2). Computations have shown that an identical nonlinear stress–strain behavior is obtained with an in-phase arrangement.[11,15]

The finite element mesh reproduces the four basic entities which influence the matrix damage evolution, i.e. the macropores, the matrix deposited on the plies (intertow matrix), the matrix infiltrated transverse and longitudinal tows (simply referred to as transverse tows or longitudinal tows in the following). For the determination of the stresses operating on the matrix, the matrix infiltrated tows are of interest. They were considered as basic entities. Their respective Young's moduli with respect to the loading direction were used for the computations, as indicated in the subsequent section.

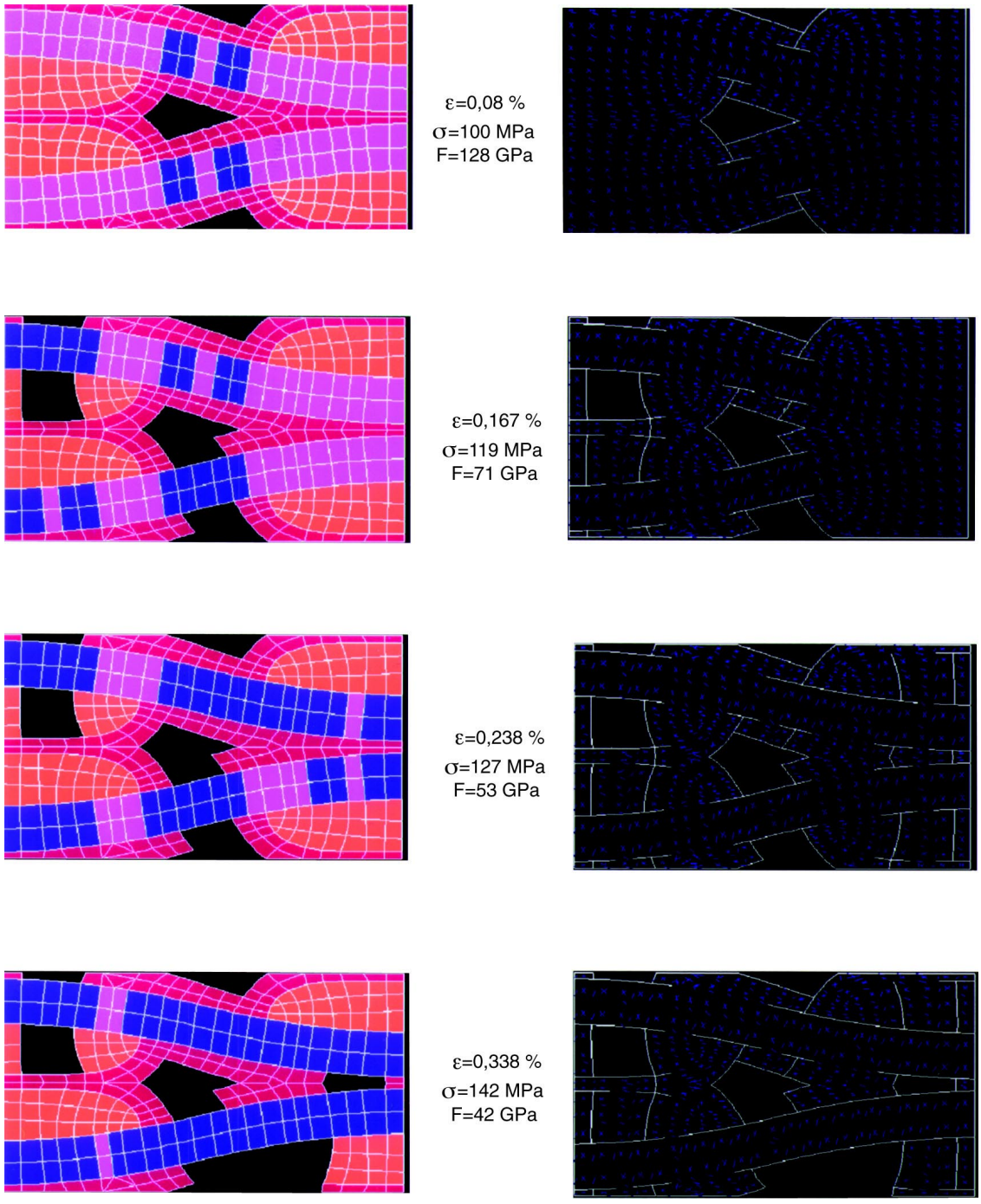

Fig. 3. Distributions of local failure probabilities and predicted damage evolution at increasing applied deformations. Also given are the resulting mean stresses and Young's moduli.

The cell of fully dense 2-D SiC/SiC did not contain the macropore. The previous mesh was used. The following boundary conditions were prescribed for the uniaxial tension (Fig. 2): (i) free displacements of faces 1 and 2 along a direction parallel to the face, (ii) uniform deformations applied to the face 3 parallel to the face 2 by 0·006% increments (deformation-based analysis).

The following boundary conditions were prescribed for the bending loading conditions: (i) free displacements in face 1 along a direction parallel to this face, (ii) no displacement at the point belonging to faces 1 and 2, (iii) non-uniform forces applied to the nodes in face 3, parallel to face 2, with a magnitude increasing linearly from 0 near face 2. Loading is described by the mean stress determined from the sum of these forces (stress-based analysis). The stress–strain curve relates this mean stress to the corresponding mean strain derived from the average of the displacements of the nodes in face 3.

2.4.2 *Properties of basic entities*

The properties of constituents required for computations are summarized in Tables 1 and 2. The Young's moduli of the transverse and longitudinal tows were estimated using the rule of mixtures as a function of surface fractions of fiber and matrix. The Young's modulus of longitudinal tows was found to be similar to that measured on individual infiltrated fiber bundles (minicomposites) tested under tension (262 GPa).[10] The fibers in the transverse tows were regarded as voids. This approximation is realistic because of the weak transverse strength of the fiber-matrix interphase.[10] The Young's modulus obtained is close to that measured by an ultrasonic technique[17] (164 GPa). The effective Young's modulus in the damaged portions of longitudinal tows was estimated from the mixture rule: $E = E_F S_F$ (where S_F is the fiber surface fraction), assuming that loads are supported only by fibers (global load sharing) and that the plies are not woven. This approximation provides a lower bound for the effective Young's modulus, thus leading to overestimated strains (in a stress-based analysis) or underestimated stresses (in as strain-based analysis). The previously mentioned work[11,15] has shown that this approximation did not affect significantly the predicted stress–strain curves which were found to be in good agreement with experimental results. The microstructure, the successive steps of matrix damage and the debond lengths at tow periphery observed on practical 2-D SiC/SiC composites were duplicated in the finite-element mesh. Poisson ratios were also estimated using the rule of mixture.

The statistical parameters required for failure probability computations have been derived from the statistical distributions of matrix strength data measured on batches of microcomposites[18] and minicomposites[10] tested individually under tension. Since the SiC matrix is obtained by chemical vapor infiltration, this is the only method to determine the statistical parameters pertinent to the CVI-SiC. One cannot fabricate test specimens of monolithic CVI-SiC.

However, this method implies the unavoidable assumption that similar flaw populations are present in the CVI-SIC matrix in the microcomposites, in the minicomposites and in the 2-D SiC/SiC composites. This assumption seems to be reasonable for the following reasons:

Table 3. Comparison of predictions and experimental results of matrix damage and corresponding applied deformations

Prediction		*Experiment*	
Deformation ε (%)	*Damage*	*Deformation* ε (%)	*Observed damage*
0·04	Crack initiation at macropore singularities	0·035	Crack initiation at macropore singularities
0·11	Crack in transverse tows	0·085	Crack in transverse tows
0·2	Cracking in longitudinal tows	0·185	Cracks in longitudinal tows

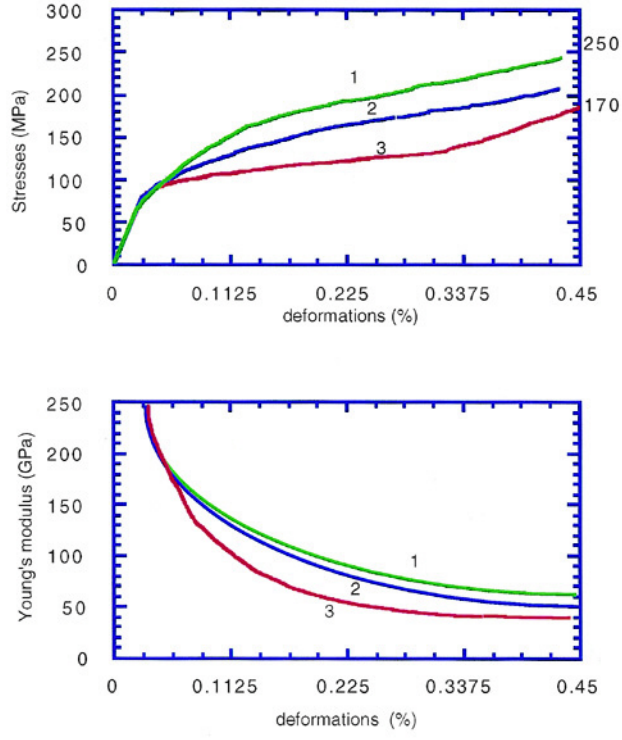

Fig. 4. Comparison of (1) experimental and (2, 3) predicted stress–strain behaviors and Young's moduli: (2) Ref. 15; (3) present analysis.

1. the microcomposites, the minicomposites and the 2-D SiC/SiC composites are fabricated using the same vapor infiltration conditions;
2. the thickness of SiC-matrix in the microcomposites, in the minicomposites and in the plies of the 2-D SiC/SiC composites is comparable (a few microns). It is slightly larger in the interply regions (about 30 μm).

The statistical parameters exhibit a certain scatter due to the presence of different residual stress fields in microcomposites and minicomposites. The statistical parameters estimated on the microcomposites were assumed to be pertinent to the intertow matrix and to the matrix in the transverse tows. Those determined on minicomposites were selected for the matrix located within the longitudinal tows.

Since the matrix infiltrated tows are treated as physical entities through homogeneized Young's moduli, the stresses in the plies that are computed (σ_c) refer to the combination of fibers and matrix.

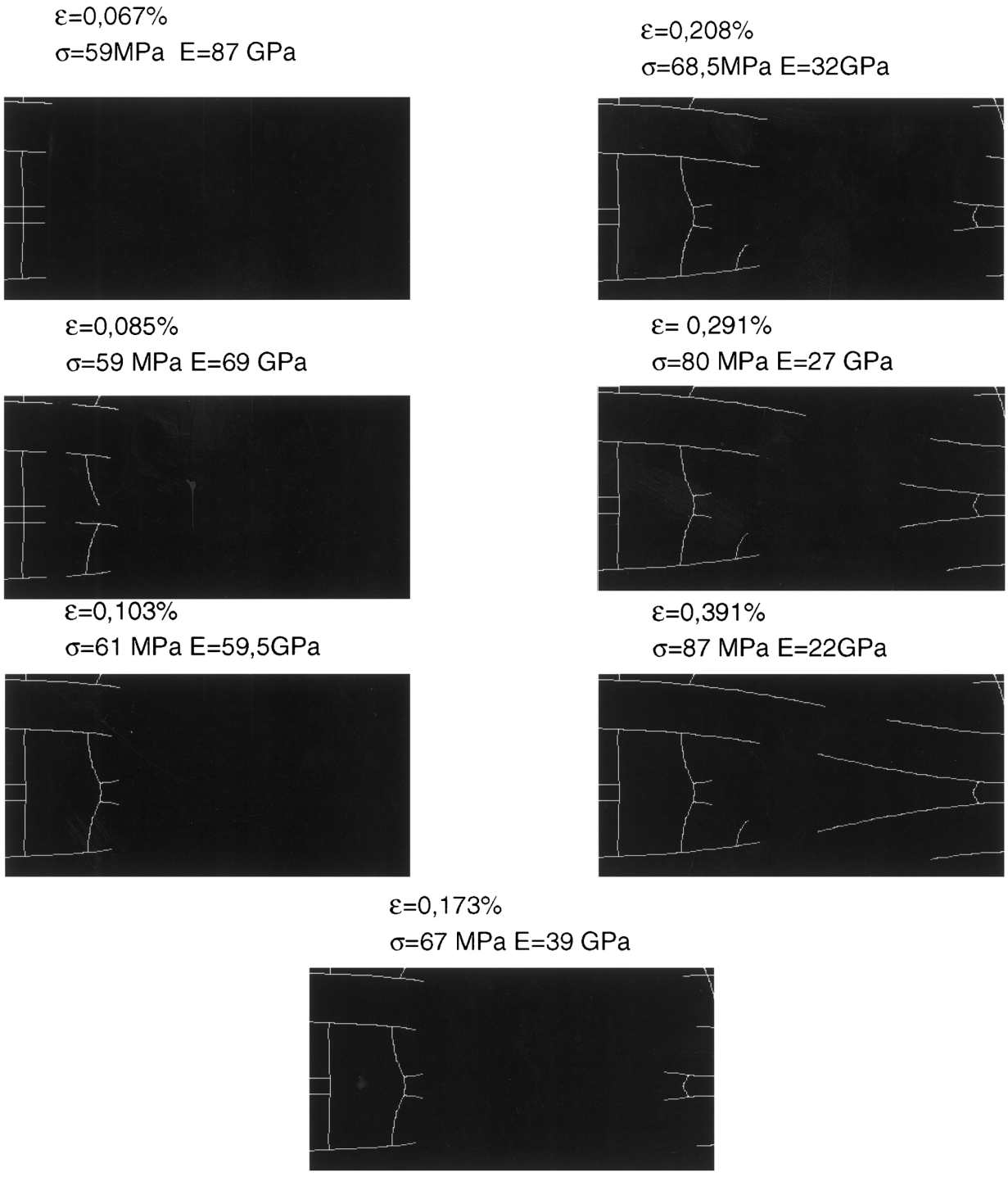

Fig. 5. Predicted damage evolution in the cell of fully dense 2-D SiC/SiC. Also given are the resulting mean stresses and Young's moduli.

For the failure probability computations, this effect was taken into account by using scale factors corrected accordingly using a constant λ defined as follows:

$$\lambda = \frac{\sigma_c}{\sigma_M} = \frac{E}{E_M} \quad (2)$$

where σ_c represents the computed stresses, σ_M the corresponding stresses in the matrix, E_M is the matrix Young's modulus, and E is the modulus of the longitudinal tows or the transverse tows. $\lambda = 0{\cdot}65$ for longitudinal tows, and $\lambda = 0{\cdot}4$ for the transverse tows.

Therefore $\lambda{\cdot}\sigma_{om}$ (σ_{om} denotes the scale factors derived from the matrix strength data distributions) was used in the failure probability computations.

Although this correction was also used in the damaged portions of the plies, it does not affect the results of the simulation since these portions are subjected to low stresses and cannot experience further damage. This was confirmed by the results of computations.

3 Results and Discussion

3.1 Simulation of matrix damage under uniaxial tension

A multiaxial non-uniform stress-state was obtained. The largest stress component is parallel to the loading direction.

Figure 3 illustrates the predicted matrix cracking evolution:

1. At a deformation of about 0·04%, cracks appear first at macropore singularities. Then they propagate across the intertow matrix to the longitudinal tows. They induce a damage in the longitudinal tows and they are deflected at the tow periphery.
2. At deformations $>0{\cdot}11\%$, cracks form within the transverse tows or in the interply matrix. The cracks propagate to the longitudinal tows. As previously, a damage is induced in the longitudinal tow, whereas crack deflection occurs at the tow periphery.
3. At deformations $>0{\cdot}2\%$, damage affects only the matrix in the longitudinal tows. This damage evolution is identical to that identified by optical microscopy on 2-D SiC/SiC test specimens after tensile tests under various prescribed strain levels[11,15] (Table 3): the three families of matrix cracks have been predicted, and the corresponding deformation thresholds are very close to the measured ones. The pertinence of the material data, and more particularly of the statistical parameters, is substantiated by this good agreement between the simulation and the experimental results.

The crack deflection at the tows periphery is satisfactorily predicted. The results thus support the criterion selected for matrix cracking. This result was expected since the multiaxial elemental strength model has proven to be appropriate for failure predictions in multiaxial stress–states.[1–4]

3.2 Stress–strain behavior and Young's moduli

Figure 4 shows that the trends predicted for the stress–strain behavior and the Young's moduli are comparable with the measurements on a 2-D SiC/SiC composite under tension. The stresses and the Young's moduli in the non-linear domain of the stress–strain curve are underestimated. This discrepancy may be attributed to various factors including matrix/tow interactions that were not prescribed, an effect of the material data selected, and a scale effect. The influence of the two dimensional cell geometry is not clear at this stage.

The tow/matrix interactions simulated are weak when compared with the practical material,[11,15] leading to a larger elongation of the tows as reflected by a larger modulus decrease. This result is

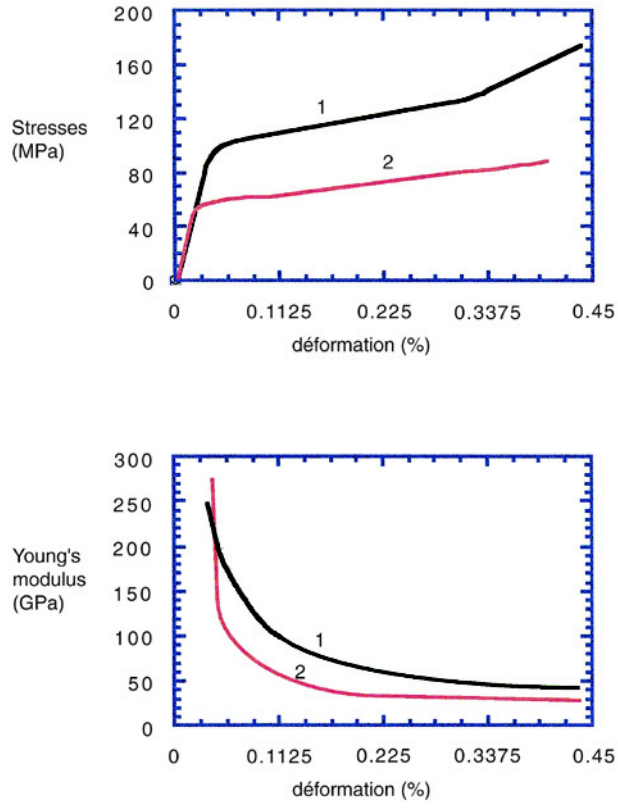

Fig. 6. Comparison of the stress–strain behaviors and the Young's moduli predicted: (1) for the conventional 2-D SiC/SiC composite, and (2) for the corresponding fully dense 2-D SiC/SiC.

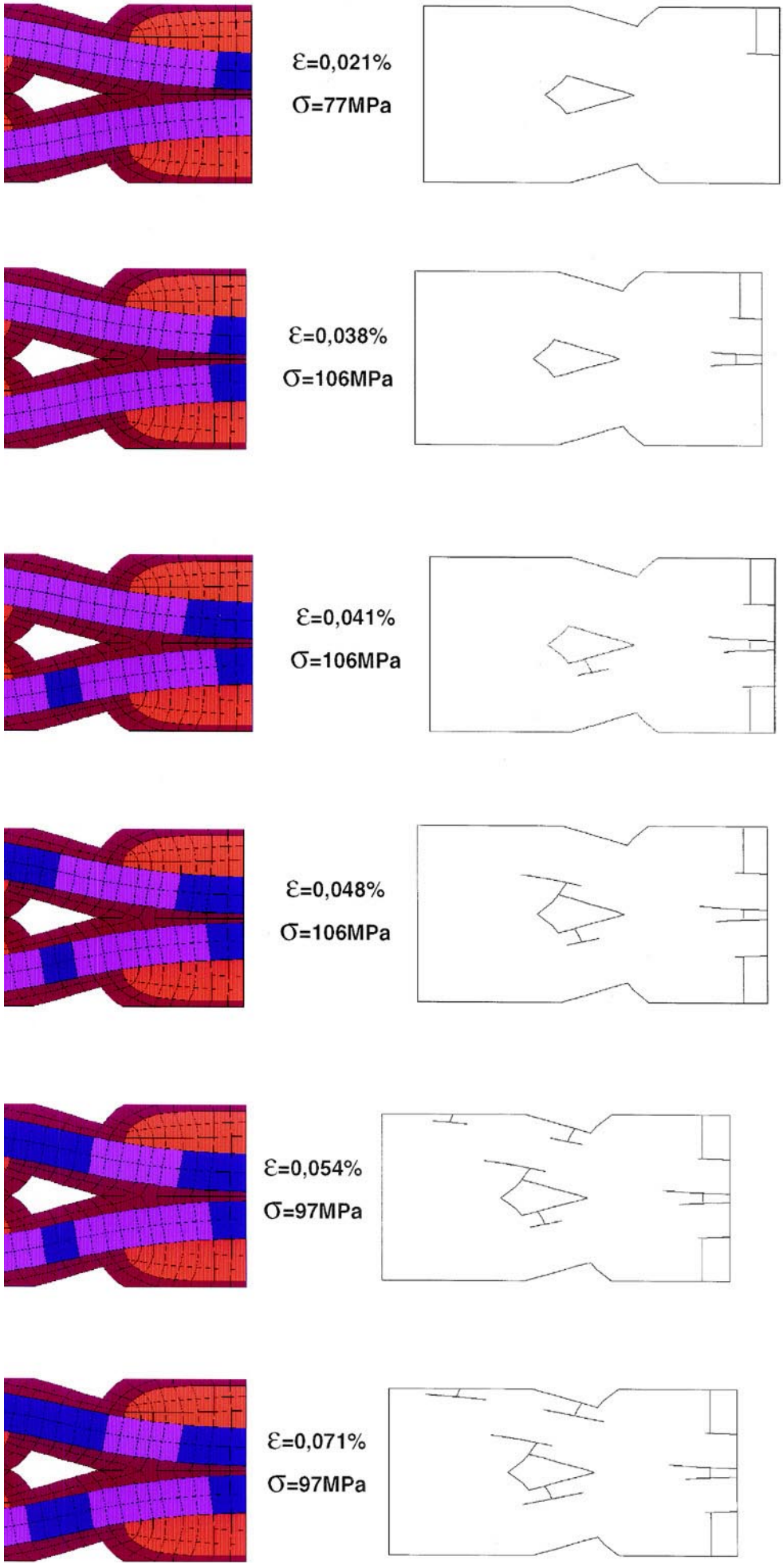
ε=0,021%
σ=77MPa
ε=0,038%
σ=106MPa
ε=0,041%
σ=106MPa
ε=0,048%
σ=106MPa
ε=0,054%
σ=97MPa
ε=0,071%
σ=97MPa

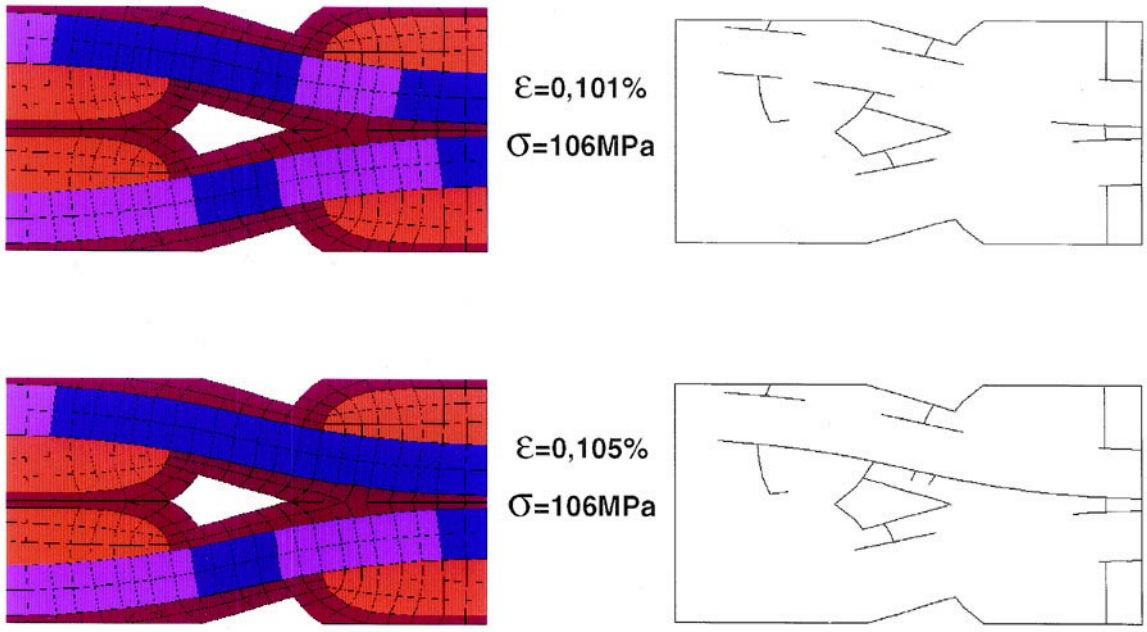

Fig. 7. Distributions of local failure probabilities and predicted damage evolution in a cell of 2-D woven SiC/SiC subject to bending forces. Also given are the mean applied stresses and the resulting mean deformations of the cell.

confirmed by Fig. 4 which shows the higher stresses and higher Young's moduli predicted in the previously mentioned work[15] which reproduced the debonds observed on practical 2-D SiC/SiC. The corresponding better agreement with experiment also suggests that the material data used in the computations are satisfactory.

However, the Young's modulus in the damaged portions of longitudinal tows may have been underestimated, particularly at the low deformations. The value derived from the mixture rule corresponds to a complete debonding, although the debonding tends to be complete at matrix cracking saturation. The curves of Fig. 4 indicate that the discrepancy between prediction and experiment diminishes as the deformation increases.

A discrepancy between the microstructures in the cell and in the practical composite may also contribute to the stress underestimation (scale effect). The cell represents an idealized microstructure with the most frequently encountered ply arrangement. The practical composite is a mosaic of cells containing different ply arrangements intermediate between the in-phase and the out-of-phase ones and macropores of various sizes. This may induce a certain variability in the degrees of damage experienced by the cells. The cell considered in the present analysis may not reproduce the average cell, but instead, the most critical one.

Finally, it cannot be concluded that the results would be improved by the use of a three dimensional analysis. It may be expected that the matrix volumes bounded by four intersecting cracks would not be more effective in the cell response if they are not be discarded, unless the fiber–matrix interactions are taken into account.

4 Applications

4.1 Fully dense 2-D woven SiC/SiC

With the exception of the cracks initiated at macropore singularities, the same families of matrix cracks as previously were predicted (Fig. 5): (i) cracks within the transverse tows or in the intertow matrix at deformations ranging between 0·04 and 0·2%, and (ii) transverse cracks in the longitudinal tows at deformations $>0{\cdot}2\%$.

Figure 6 illustrates the influence of the presence of macropores upon the stress–strain behavior and the Young's moduli. The lower stress and Young's modulus at a given deformation are displayed by the fully dense SiC/SiC. As logically expected, the initial Young's modulus of the fully dense SiC/SiC is significantly larger (275 GPa) than that one pertaining to the conventional SiC/SiC (247 GPa). Furthermore, it is very close to the value given by the mixture rule (272 GPa).

Comparison of the matrix cracking evolution in both types of cell evidences the following features that explain the stress–strain behavior of the fully dense composite with respect to the conventional one:

1. matrix cracking initiates at the same deformation of 0·04% in both cases;
2. the pattern of long transverse cracks crossing the transverse tows is observed in both cases,

but it appears at lower deformations in the fully dense material. These cracks are observed from a deformation of 0·04% in the fully dense composite, and from a deformation of 0·1% in the conventional one. As logically expected, the corresponding Young's moduli are comparable (respectively, 87 and 88 GPa). Then, the two long transverse cracks close to the face 1 that are predicted at a deformation of 0·085% in the fully dense composite, appear at a deformation of 0·17% in the conventional composite. Again, the corresponding Young's moduli are similar (respectively, 69 and 71 GPa). Therefore, at a given deformation, the fully dense composite experiences the more severe damage consisting of the long transverse cracks. By comparison, the cracks initiated by the macropores are much shorter, and consequently they are less detrimental.

As previously for the conventional composite, no specific condition was prescribed to the tow/matrix interactions. Therefore, the interactions may be considered to be comparable in both composites.

The predicted favorable influence of macropores may be related to the relaxation of stresses in the intertow matrix and in the transverse tows, as indicated by the stress analysis. In the fully dense composite, the peak stresses are located in the narrow strip of intertow matrix close to the face 1, whereas the regions corresponding to the location of the macropores are subject to lower stresses. Furthermore, the transverse tows are subject to high stresses when comparing with the conventional composite. In the conventional composite, the stress magnitude at a macropore angle is around 300 MPa (at a deformation of 0·035%), for the mesh elements selected. However, because of the shape of the pore, a moderate stress concentration must be expected. This is supported by the comparison with experimental results which showed an excellent prediction of the proportional limit (Table 3). The peak stresses in the fully dense composite are not several orders of magnitude smaller than the stress at a macropore angle (around 190 MPa at a deformation of 0·035%). This is consistent with the initiation of the first cracks at the same applied deformation in both composites.

Experimental data on a fully dense 2-D SiC/SiC are not available, since this composite cannot be fabricated for practical reasons. However, the results seem to be realistic.

4.2 Bending of a cell of conventional 2-D woven SiC/SiC

Figure 7 shows that the matrix cracking evolution is dominated by debonding, whereas the number of transverse cracks is limited. Thus, the first transverse crack initiates in the transverse tows and in the intertow matrix close to the loaded surface (face 3) at a small deformation of about 0·02%. At higher deformations, additional transverse cracks appear in the intertow matrix located in the macropore area, and then, near the outer surface (face 4). These cracks propagate to the nearest longitudinal tow which experiences damage. Then, only the associated debonding cracks grow (at deformations $>0{\cdot}1\%$). The debonding cracks coalesce. The behavior of the cell becomes dictated by the longitudinal tows when the debonding is complete. The computations stop at this stage.

The stress–strain curve exhibits three domains (Fig. 8) which reflect the initial elastic response of the cell, and then the above damage: transverse cracking (deviation to linearity), and debonding (deformation at a constant force). This curve reproduces the trends observed in the mechanical behavior measured on the practical 2-D SiC/SiC under three-point bending conditions (Fig. 9).

A quantitative comparison of both curves cannot be done, since the predicted stress–strain curve refers to the mean stresses and strains in a cross section of the cell, whereas the curve of Fig. 9 relates the applied force to the strains measured in the outer surface of the specimen.

Furthermore, it is worth pointing out that this analysis was not aimed at simulating the mechanical behavior of the SiC/SiC composite during a three-point bending test, but instead at illustrating the potential of the approach. The cell does not represent a part of a three-point bending test specimen. The boundary conditions may not be consistent with the stresses induced in a test specimen. The important result is that the proposed approach predicted the mode of damage (dominated by debonding) which has been observed in 2-D woven SiC/SiC composites, and more generally, in

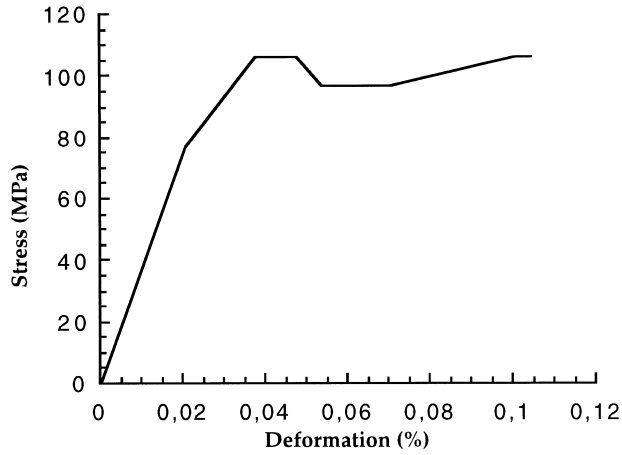

Fig. 8. Predicted stress–strain behavior for the cell of 2-D woven SiC/SiC subjected to bending forces.

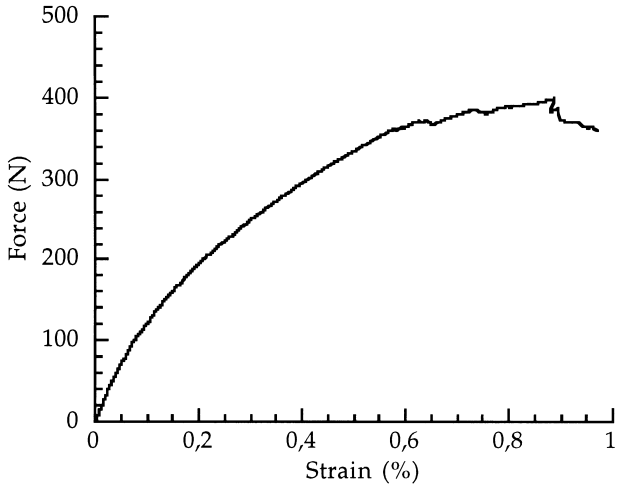

Fig. 9. Force-deformation behavior of the 2-D woven SiC/SiC composite during a three-point bending test.[19]

laminated CMCs in bending.[11,19–21] Quantitative correlations with a three-point bending specimen require that the boundary conditions reproduce the stress–state operating in the test specimen.

5 Concluding Remarks

Matrix cracking in a 2-D woven SiC/SiC composite was simulated from properties of basic constituents on the basis of failure probability computations.

The damage evolution predicted was found to be in excellent agreement with that identified on practical 2-D woven SiC/SiC composites under a uniaxial tensile load. The predicted stress–strain curves and Young's modulus compared satisfactorily with experimental data. However a certain discrepancy was observed which was attributed primarily to the matrix/tow interactions.

Then, this approach was applied to predict the damage evolution and the stress–strain behavior of a fully dense 2-D woven SiC/SiC composite. The results indicated that the macropores have a beneficial effect on the mechanical behavior. The short macropore-induced cracks are less detrimental than the long transverse cracks that would appear in the fully dense SiC/SiC.

Finally, the potential of this approach to handle complex loading conditions was illustrated on a cell subjected to non-uniform forces. The approach predicted the damage evolution (involving intense debonding) observed on practical CMCs under bending conditions. The stress–strain curve exhibited the features of the mechanical behavior evidenced on the practical 2-D woven SiC/SiC composite.

Refinements are envisaged to take into account tow/matrix interactions. However, the results of this analysis indicate that this approach may be used to simulate matrix damage and related stress–strain behavior from properties of basic constituents, for any composite microstructure.

Acknowledgements

The authors acknowledge support of SEP and CNRS.

References

1. Lamon, J. and Evans, A. G., Statistical analysis of bending strengths for brittle solids: a multiaxial fracture problem. *J. Am. Ceram. Soc.*, 1983, **66**(3), 177–182.
2. Lamon, J., Statistical approaches to failure for ceramic reliability assessment. *J. Am. Ceram. Soc.*, 1988, **71**(2), 106–112.
3. Lamon, J., Ceramics reliability: statistical analysis of multiaxial failure using the Weibull approach and the Multiaxial Elemental Strength model. *J. Am. Ceram. Soc.*, 1990, **73**(8), 2204–2212.
4. Lamon, J., Probabilistic failure predictions in ceramics and ceramic matrix fiber reinforced composites. In *Life Predictions Methodologies and Data for Ceramic Materials* ASTM STP 1201, ed. C. P. R. Brinkman and S. F. Duffy. American Society for Testing and Materials, Philadelphia, PA, 1994, pp. 265–279.
5. Curtin, W. A., Theory of mechanical properties of ceramic matrix composites. *J. Am. Ceram. Soc*, 1991, **74**(11), 2837–2845.
6. Steif, P. S. and Schwietert, H. R., Ultimate strength of ceramic matrix composites. *Ceram. Eng. Sci. Proc*, 1990, **11**(9–10), 1567–1576.
7. Sutcu, M., Weibull statistics applied to fiber failure in ceramic composites and work of fracture. *Acta Metall*, 1989, **37**, 2567–2583..
8. Cao, H. and Thouless, M. D., Tensile tests on ceramic-matrix composites: theory and experiment. *J. Am. Ceram. Soc.*, 1990, **73**(7), 2091–2094.
9. Guillaumat, L. and Lamon, J., Fracture statistics applied to modelling the nonlinear stress–strain behavior in microcomposites: influence of interfacial parameters. *Int. J. of Fracture*, 1996, **82**, 297–316.
10. Lissart, N. and Lamon, J., Damage and failure in ceramic matrix minicomposites: exprimental study and model. *Acta Mater*, 1997, **45**, 31025–3044.
11. Guillaumat, L., Microfissuration des CMC: relation avec la microstructure et le comportement mécanique (Multiple microcracking in CMCs: relationships with microstructure and mechanical behavior). Ph.D. thesis, University of Bordeaux, France, 1994.
12. Kuo, W. S. and Chou, T. W., Modelling of non-linear constitutive relations of woven ceramic composites. *Ceram. Eng. Sci. Proc*, 1991, **12**, 1556–1573.
13. Dumont, J. P., Ladevèze, M. Poss, and Y. Remond. Damage Mechanics for 3D composites. *Comp. Struct.*, 1987, **8**, 119–141.
14. Aubard, X., Lamon, J. and Allix, O., Model of the nonlinear mechanical behavior of 2D SiC–SiC CVI composites. *J. Am. Ceram. Soc.*, 1994, **77**(8), 2118–2126.
15. Guillaumat, L. and Lamon, J., Probabilistic-statistical simulation of the nonlinear mechanical behavior of a woven SiC/SiC composite. *Comp. Sc. Tech.*, 1996, **56**, 803–808.
16. Lamon, J., Probabilistic failure predictions in brittle materials under multiaxial loading. In *Probabilities and Materials*, ed. D. Breysse Kluwer Academic, Dordrecht, The Netherlands, 1994, pp. 415–426.

17. Baste, S., Gerard, A. and Roux, J., Modélisation et mesure ultrasonore de I'endommagement anisotrope (Modelling and ultrasonic measurement of anisotropic damage). In *Revue des Composites et des Matériaux Avancés,* Vol. 3, numéro hors série, ed. J. L. Chermant and G. Fantozzi. Hermès, Paris, 1993, pp. 129–144.
18. Lamon, J., Lissart, N., Rechigniac, C., Roach, D. M. and Jouin, J. M., Micromechanical and statistical approach to the behavior of CMCs. *Proceedings of the 17th Annual Conference on Composites and Advanced Ceramics, Cocoa Beach, FL*, September–October 1993. The American Ceramic Society, Westerville, OK, pp. 1115-1124.
19. Calard, V. and Lamon, J., unpublished work.
20. Phillips, A. J., Clegg, W. J. and Clyne, T. W., Fracture behaviour of ceramic laminates in bending–1. Modelling of crack propagation. *Acta Metall. Mater*., 1993, **41**(3), 805–817.
21. Morrell, R. and McCartney, L. N., Measurement of properties of brittle matrix composites. *Brit. Ceram. Trans*., 1993, **92**(1), 1–7.